

CONDENSED MATTER PHYSICS

Unusual behavior of cuprates explained by heterogeneous charge localization

D. Pelc^{1,2}, P. Popčević^{3,4}, M. Požek^{1*}, M. Greven^{2*}, N. Barišić^{1,2,3*}

The discovery of high-temperature superconductivity in cuprates ranks among the major scientific milestones of the past half century, yet pivotal questions regarding the complex phase diagram of these materials remain unanswered. Generally thought of as doped charge-transfer insulators, these complex oxides exhibit pseudogap, strange-metal, superconducting, and Fermi liquid behavior with increasing hole-dopant concentration. Motivated by recent experimental observations, here we introduce a phenomenological model wherein exactly one hole per planar copper-oxygen unit is delocalized with increasing doping and temperature. The model is percolative in nature, with parameters that are highly consistent with experiments. It comprehensively captures key unconventional experimental results, including the temperature and the doping dependence of the pseudogap phenomenon, the strange-metal linear temperature dependence of the planar resistivity, and the doping dependence of the superfluid density. The success and simplicity of the model greatly demystify the cuprate phase diagram and point to a local superconducting pairing mechanism.

INTRODUCTION

The parent cuprate compounds are antiferromagnetic charge-transfer insulators that evolve into conductors and superconductors upon doping. The superconducting transition temperature is highest at an optimal level of $p \approx 0.16$ doped holes per planar CuO_2 unit, and therefore, the phase diagram is divided into underdoped and overdoped regions. The highly overdoped materials behave as conventional Fermi-liquid metals, with a large Fermi surface that corresponds to $1 + p$ holes per CuO_2 unit and a planar resistivity that exhibits quadratic temperature dependence (*1*). The underdoped region features the pseudogap regime below a characteristic temperature T^* that decreases linearly with doping and extrapolates to zero around $p_c \approx 0.20$ (*1*). The pseudogap is associated with a depletion of electronic states at the Fermi level and with myriad charge and magnetic ordering tendencies. Above T^* , in the unusual “strange-metal” regime, the resistivity is approximately linear in an extended temperature range.

Recent transport and optical conductivity experiments revealed that the itinerant carriers below a characteristic temperature $T^{**} < T^*$ behave like a Fermi liquid (*2–7*), with a carrier density that is equal to the nominal concentration p . The itinerant carrier concentration therefore evolves from p in the pseudogap regime to $1 + p$ in the overdoped regime. As would be expected from these observations, the inverse Hall mobility [i.e., the cotangent of the Hall angle, $\cot(\Theta_H)$], a measure of the transport scattering rate, also exhibits Fermi-liquid behavior below T^{**} . The quadratic temperature dependence of $\cot(\Theta_H)$ continues uninterrupted beyond T^* , into the strange-metal regime, with virtually no doping or compound dependence (*5, 6*). These observations constitute a crucial constraint that has not been captured theoretically. Interpreted in the simplest possible manner (*5*), the transport data imply that the carrier density acquires temperature dependence in the strange-metal regime and that the same underlying Fermi-liquid physics describes the itinerant carriers throughout the entire phase diagram.

¹Department of Physics, Faculty of Science, University of Zagreb, Bijenička cesta 32, HR-10000 Zagreb, Croatia. ²School of Physics and Astronomy, University of Minnesota, Minneapolis, MN 55455, USA. ³Institute of Solid State Physics, TU Wien, 1040 Vienna, Austria. ⁴Institute of Physics, HR-10000 Zagreb, Croatia. *Corresponding author. Email: mpozek@phy.hr (M.P.); greven@umn.edu (M.G.); neven.barisic@tuwien.ac.at (N.B.)

A second ubiquitous feature of the cuprates is structural and electronic inhomogeneity on multiple length scales (*8–11*). Surface-sensitive probes such as scanning tunneling microscopy (STM) (*12*) reveal broad distributions of local electronic gaps, and bulk local probes such as nuclear magnetic resonance (NMR) (*13*) provide evidence of intrinsic electrostatic inhomogeneity. Recent conductivity and magnetization experiments show that the superconducting precursor regime is dominated by inhomogeneity, leading to percolation (*14–16*). Yet, inhomogeneity is often disregarded in modeling the salient features of the cuprates.

Here, we present a phenomenological model of the cuprate phase diagram that respects the experimental observation of universal underlying Fermi-liquid behavior and combines it with spatially inhomogeneous (de)localization-induced changes in the itinerant hole density. The model does not involve specific assumptions about microscopics but rather provides a broad framework to understand the cuprates, and it parametrizes their common behavior with a small number of experimentally constrained constants. The model is thus comparable to well-known phenomenological approaches in science, such as the Standard Model of particle physics, the Landau theory of phase transitions, and models of population growth. Along with a comprehensive description of the normal state, our model gives fresh insight into key aspects of the superconducting state that are at odds with existing theories, and it therefore paves the way toward a microscopic understanding of cuprate superconductivity. In particular, we show that the unexpected decrease of the superfluid density in the overdoped part of the phase diagram (*17*) follows naturally if we simply assume that the pairing glue is associated with the localized holes. The superfluid density is thus obtained from the evolution of the normal-state properties.

The model

The above-listed experimental facts provide the foundation of our model, leading to three general premises. First, two electronic subsystems coexist within the unit cell: itinerant and localized holes, with the p holes introduced via doping always being itinerant. Along with the aforementioned transport and optical experiments (see the Supplementary Materials) (*18*), local-probe evidence for the two components comes from NMR (*19, 20*), and specific heat results are consistent with

Copyright © 2019
The Authors, some
rights reserved;
exclusive licensee
American Association
for the Advancement
of Science. No claim to
original U.S. Government
Works. Distributed
under a Creative
Commons Attribution
NonCommercial
License 4.0 (CC BY-NC).

Downloaded from <http://advances.sciencemag.org/> on May 11, 2020

this scenario (21). Second, we use the experimental fact that the itinerant component exhibits a universal Fermi-liquid transport scattering rate throughout the phase diagram (5, 6). The third premise is that the localized subsystem consists of exactly one hole per CuO_2 unit, separated from the Fermi level by a spatially inhomogeneous, doping-dependent localization gap Δ (11, 12). In photoemission experiments, this is manifested as a partially gapped Fermi surface that is repopulated from arcs to the full carrier density of $1 + p$ with increasing doping as the individual gaps close with doping, there is no essential change in the shape of the underlying Fermi surface (22). The states on the arcs therefore are exactly the same as those found at high doping levels (5), where a Fermi liquid exists. We associate the localization gap with the strong electronic correlations that cause the charge-transfer gap of the undoped parent insulators. As itinerant carriers are introduced into the material, they are expected to influence the electronic interactions. The gap should therefore decrease with doping and, eventually, close beyond optimal doping, where the carrier density approaches $1 + p$. Moreover, the gap is taken to be inhomogeneous, i.e., to vary from one CuO_2 unit to another, again in line with experiments. To examine the predictions of the model, we quantify the above statements in the simplest possible manner. The basic quantity is the effective density $p_{\text{eff}}(p, T)$ of itinerant carriers, which depends on temperature and doping. Doping provides p itinerant carriers per per CuO_2 unit. Each CuO_2 unit also contains one localized hole that can be thermally activated, giving rise to an $e^{-\Delta/2kT}$ term ($k = 1.38 \times 10^{-23}$ J/K is the Boltzmann constant). Once the local gap Δ closes, the corresponding hole is

added to the Fermi sea. Since the gap is inhomogeneous, the effective hole density is

$$p_{\text{eff}}(p, T) = p_{\text{eff}}(p, 0) + \int_0^{\infty} g(\Delta) e^{-\Delta/2kT} d\Delta \quad (1)$$

where $p_{\text{eff}}(p, 0)$ is the effective density at zero temperature and $g(\Delta)$ is the doping-dependent normalized gap distribution function. We start by considering a simple Gaussian function for the distribution of local environments, with a doping-independent width δ and a mean Δ_p that decreases linearly with doping, $\Delta_p = \Delta_0 (1 - p/p_c)$, where Δ_0 and p_c are constants. Our results are not very sensitive to the precise choice of the distribution function or to the form of its doping dependence (see extended discussion in the Supplementary Materials). The portion of the Gaussian with nominally negative gaps simply represents those CuO_2 units whose gaps have closed and thus have their holes added to the Fermi sea (Fig. 1A). The effective density at zero temperature then is simply

$$p_{\text{eff}}(p, 0) = p + \int_{-\infty}^0 g(\Delta) d\Delta \quad (2)$$

The thermal activation term is approximate, since it assumes a constant prefactor (of unity), whereas the true density of states may be temperature dependent. We note that the same form was used in previous analyses of the Hall density (23, 24), and we use it for simplicity. Equation 1 has physically compelling limits: p_{eff} is $1 + p$ both at high

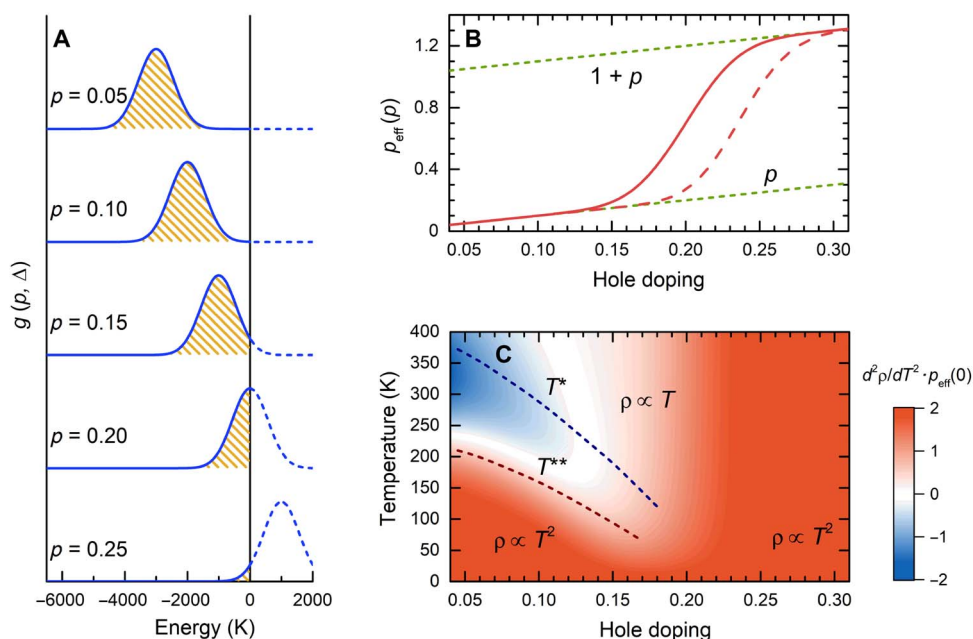


Fig. 1. Gap inhomogeneity and phase diagram of the cuprates. (A) Gaussian gap distribution function g at several doping levels, shown as a function of energy. The parameters are $p_c = 0.2$, $\Delta_0 = 4000$ K, and $\delta = 800$ K. The fraction of the distribution that has reached the Fermi level (the portion above zero energy indicated with a dashed line) is added to the p delocalized doped charge carriers at temperature $T = 0$. (B) Effective density of delocalized carriers per CuO_2 unit at $T = 0$, obtained as the sum of the doped hole concentration p and delocalized holes from the distributions shown in (A) (full line). The dashed line corresponds to the (skewed Gaussian) gap distribution parameters used for comparison with experiments on $\text{La}_{2-x}\text{Sr}_x\text{CuO}_4$ [LSCO; see Figs. 2 (C and D) and 4, Materials and Methods, and Supplementary Materials], with $p_c = 0.22$, $\Delta_0 = 3900$ K, $\delta = 800$ K, and skew parameter $\alpha = 2$. (C) Second derivative of the normal-state resistivity, multiplied by p_{eff} at $T = 0$. This result is obtained by combining the effective carrier density from Eq. 1, obtained with the gap distributions in (A), with the experimentally determined Fermi liquid scattering rate of itinerant carriers (5). The characteristic features of the phase diagram are apparent: a quadratic resistive regime at both low and high doping, the temperatures T^{**} and T^* , and the linear- T -like regime around optimal doping.

temperatures and high doping levels. Furthermore, the density of localized holes is $p_{\text{loc}} = 1 + p - p_{\text{eff}}$.

Neglecting compound-specific Fermi-surface complications that can cause a failure of the effective-mass approximation but not of the applicability of Fermi-liquid concepts (see the Supplementary Materials) (5), we take $\rho = C_2 T^2 / p_{\text{eff}}$ and $R_H = 1 / (e p_{\text{eff}})$ for the resistivity and Hall constant (per CuO_2 unit), respectively. Notably, the universal temperature dependence $\cot(\Theta_H) = C_2 T^2$ is embedded in these calculations, i.e., the experimentally established value $C_2 = 0.0175 \text{ K}^{-2}$ (5, 6) is used to obtain the absolute value of ρ . We note that this experimental value is consistent with estimates for conventional Umklapp electron-electron scattering (25, 26).

We model the superfluid density ρ_{s0} by assuming that pairing only occurs in the vicinity of localized holes

$$\rho_{s0} = \gamma \sigma_{\text{dc}}^{\text{res}} T_c p_{\text{loc}} = \rho_{s0}^{\text{H}} p_{\text{loc}} \quad (3)$$

This expression consists of two parts: (i) the conventional dirty Bardeen-Cooper-Schrieffer (BCS) expression for itinerant holes (Homes' law) (27), $\rho_{s0}^{\text{H}} = \gamma \sigma_{\text{dc}}^{\text{res}} T_c$, where $\gamma = 35.2 \text{ cm/K-microhm}$ is a universal numerical constant, T_c is taken as a measure of the superconducting gap as per BCS theory, and $\sigma_{\text{dc}}^{\text{res}}$ is the residual normal-state conductivity, a measure of (pair-breaking) disorder; (ii) p_{loc} , obtained directly from modeling the normal state. The simplest possible, linear dependence is assumed between ρ_{s0} and p_{loc} . Homes' law fails to give the correct dependence of ρ_{s0} on doping (or T_c) for overdoped compounds (17). Note also that Homes' law breaks down in the limit of low levels of pair-breaking (point) disorder (27), which some cuprates, such as $\text{HgBa}_2\text{CuO}_{4+\delta}$ (Hg1201), might approach.

Modification of the model at low superfluid densities

In a local pairing scenario with short coherence lengths and underlying spatial inhomogeneity, superconducting gap inhomogeneity should also play an important role when bulk superconductivity is not fully established. It was recently shown (for $p < p_c$) that superconductivity appears in a percolative fashion upon cooling toward T_c (14–16). The underlying inhomogeneity induces a superconducting gap distribution of nearly universal width $\Xi_0 \sim 30 \text{ K}$. Close to the critical doping levels $p_{c1} \approx 0.06$ and $p_{c2} \approx 0.26$ that define the zero-temperature extent of the bulk superconducting state, we thus expect the simple relation Eq. 3 to be modified by a percolative term. We will show that this provides an excellent description of the superfluid density near p_{c2} .

RESULTS

Figure 1 shows a generic calculation with a Gaussian distribution with $p_c = 0.2$, $\Delta_0 = 4000 \text{ K}$, and $\delta = 800 \text{ K}$ (Fig. 1A). The density of itinerant holes at $T = 0$ obtained from Eq. 1 is shown in Fig. 1B: $p_{\text{eff}}(T = 0)$ begins to deviate from p around optimal doping and smoothly crosses over to $1 + p$ holes at high doping/temperature. Motivated by experimental work (7), the temperature and doping dependence of the resistivity curvature, $d^2\rho/dT^2 \cdot p_{\text{eff}}(T = 0)$, is plotted to obtain the phase diagram in Fig. 1C. All defining normal-state features are captured as follows: the T^2 regime in the underdoped region that ends at T^{**} ; the characteristic temperature T^* ; an extended linear- T -like regime around optimal doping; and a smooth crossover to Fermi-liquid behavior on the overdoped side. This is achieved with a mere three param-

eters with values consistent with experiments: δ is consistent with the widths of features seen in optical conductivity and STM (figs. S3 and S4) (18, 28), p_c is roughly the doping level where T^* extrapolates to zero, and Δ_0 is broadly consistent with the charge-transfer gap scale (24). As noted, an additional parameter, the experimentally determined universal scattering-rate coefficient C_2 , is needed to obtain numerical values of the resistivity (5, 8). The results are not sensitive to details of the distribution shape (see the Supplementary Materials).

Figure 2 demonstrates excellent quantitative agreement of the model with transport data for Hg1201 and $\text{La}_{2-x}\text{Sr}_x\text{CuO}_4$ (LSCO). Motivated by STM and nuclear quadrupole resonance work (see the Supplementary Materials and fig. S3) (12, 13), we use a slightly different, skewed Gaussian gap distribution, although the generic Gaussian (Fig. 1) leads to similar results (see the Supplementary Materials and figs. S1 and S2). Figure 2 (A and B) shows the resistivity and Hall constant of underdoped Hg1201 (5) along with the model results. The doping level ($p \approx 0.1$) was chosen because all characteristic features are observed there, including T^{**} , T^* , and the linear- T resistivity regime. Figure 2 (C and D) demonstrates that the model captures the doping and temperature dependence of the resistivity curvature of LSCO. It also captures the “anomalous criticality” observed in the resistivity above optimal doping (fig. S7) (29), the temperature dependence of the Hall constant at all doping levels (fig. S6) (23), and the universal dependence of the linear and quadratic sheet resistance coefficients on doping (fig. S8) (2).

Charge transport is a good probe of the itinerant subsystem, since it is sensitive to an energy window $\sim kT$ around the Fermi level, yet it is only an indirect probe of the localized-carrier subsystem below the Fermi level. More detailed insight into energy scales related to the charge-transfer gap can be obtained from spectroscopic techniques, and we compare our model to these results. Experimental signatures of the gap scale (see the Supplementary Materials) (11, 18) include broad features in tunneling and photoemission spectroscopy, as well as a characteristic mid-infrared peak in optical spectroscopy (fig. S4). As shown in Fig. 3, the agreement between the model parameters obtained from transport and the spectroscopic techniques is remarkable in the superconducting doping range ($p > 0.05$). Not surprisingly, at low doping, a simple linear doping dependence of the mean gap scale is inadequate, as it extrapolates to a value that is substantially smaller than the charge-transfer gap (24). To correct for this deviation, in agreement with spectroscopic results, alternative parametrizations of the doping dependence are possible (see Materials and Methods) that extrapolate to the correct charge-transfer gap value and yield even better agreement with transport results. Microscopically, the nonlinear dependence is expected, since the gap decreases because of the influence of the itinerant subsystem, and the density of itinerant holes, in turn, depends on the value of the mean gap.

Once the gap distribution parameters are known for the normal state, the superfluid density naturally follows—crucially, no additional free parameters are introduced (except for the description of the narrow region close to p_{c2} ; see below). To calculate ρ_{s0} for LSCO we approximate $\sigma_{\text{dc}}^{\text{res}}$ in Eq. 2 by a small constant in the overdoped regime [$1/\sigma_{\text{dc}}^{\text{res}} = 15 \text{ microhm-cm}$, consistent with experiments (7, 29)], use doping-dependent values of $\sigma_{\text{dc}}^{\text{res}}$ from experiment below optimal doping (7), and calculate p_{loc} from Eq. 1. As shown in Fig. 4, the result of this calculation is in excellent agreement with the experimentally determined doping dependence of ρ_{s0} . On the overdoped side, ρ_{s0} is limited by p_{loc} , whereas on the underdoped side, $p_{\text{loc}} = 1$, and Homes' law is recovered.

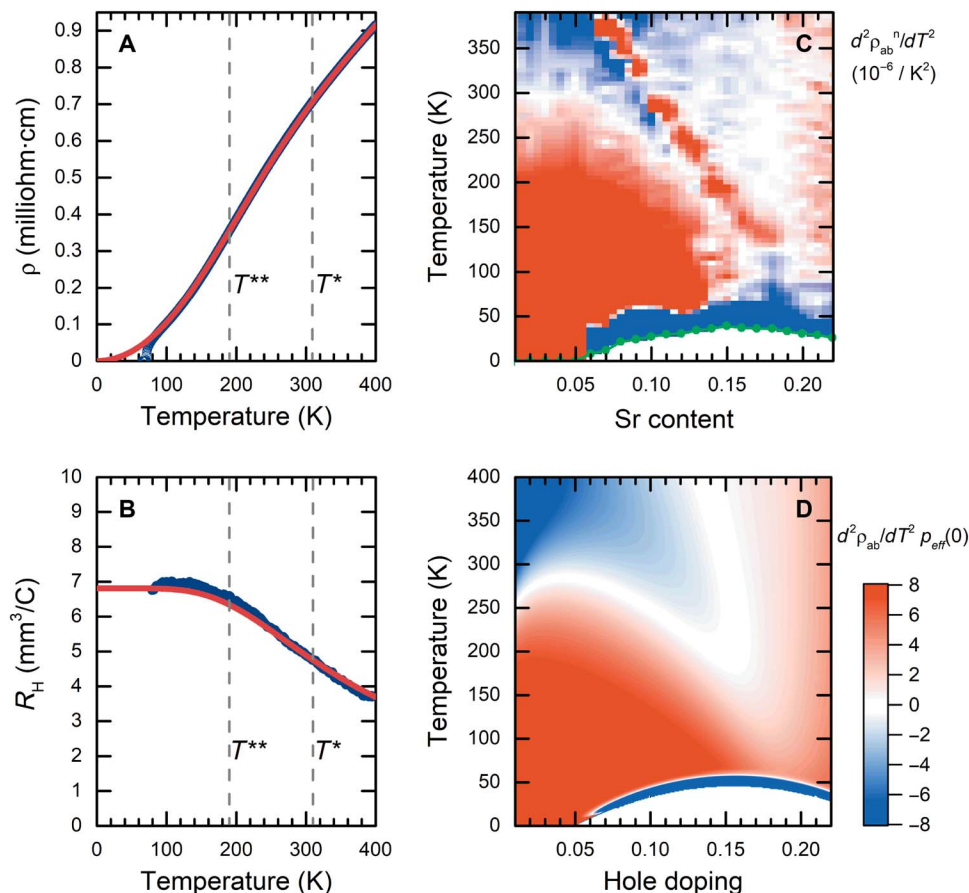


Fig. 2. Comparison of the model to experiments. (A) Resistivity and (B) Hall constant for underdoped Hg1201 [$p \approx 0.1$; blue circles; data from (5)] compared with the gap disorder model (red lines). A skewed Gaussian gap distribution and linear mean gap doping dependence are used, with $p_c = 0.2$, $\Delta_0 = 4000$ K, $\delta = 600$ K, and $\alpha = 2$ (see Materials and Methods). The asymptotic value of the measured R_H at $T = 0$ corresponds to $\sim 90\%$ of the nominal concentration of itinerant carriers, and the calculated curve is thus multiplied by the same factor. Note that this value is within the experimental uncertainty due to sample size and shape uncertainty (2, 5). (C) Resistivity curvature map of LSCO normalized at each doping level to $\rho(300$ K), from (7). In addition to the characteristic temperatures T^{**} and T^* , LSCO features a structural transition, which is detected in the resistivity measurement (red downward sloping line) (5). (D) Calculated resistivity curvature map, with added percolative superconducting precursor regime (14) close to T_c and parameters $p_c = 0.22$, $\Delta_0 = 3900$ K, $\delta = 800$ K, and $\alpha = 2$ (same as for the dashed line in Fig. 1B). Resistivity is normalized by $\rho_{eff}(T = 0)$, which is nearly equivalent to the experimental normalization and multiplied by a factor of $4 \cdot 10^{-6}$ to have the same absolute color scale as (C).

As noted, in the narrow regions at the edges of the superconducting dome, Eq. 3 ought to be modified by a percolative correction due to intrinsic superconducting gap disorder. We take this corrective term from previous work on granular superconductors (see Materials and Methods) and use the detailed measurements of $\rho_{s0}(p)$ for overdoped LSCO (17) to test this idea. As seen from Fig. 4B, we again find excellent quantitative agreement with experiments: The model captures the kink at $T_c \sim 12$ K and, in particular, the low- T_c regime is consistent with superconducting percolation scaling. We emphasize that this scaling, $\rho_{s0} \sim T_c^{1.6}$, directly follows from the data of (17) and, hence, constitutes independent support for percolation (note that it is independent of the particular model for the percolation correction). The width of the superconducting gap distribution, Ξ_0 , is introduced as a free parameter, and the data are best fit with $\Xi_0 = 23 \pm 1$ K, remarkably close to the value 27 ± 2 K obtained in previous studies of the superconducting precursor as a function of temperature (14, 16). Alternatively, no additional free parameter is necessary if we take this previous result as input, and we achieve nearly the same good agreement in the percolation regime. Signatures of granular superconductivity

have also been observed (30) in experiments on underdoped thin films of $\text{YBa}_2\text{Cu}_3\text{O}_{6+\delta}$ (YBCO), which mirror the percolative regime discussed here.

DISCUSSION

Our minimalistic phenomenological model captures both the normal- and superconducting-state behavior at a quantitative level, yet it provides neither the microscopic origin of the inhomogeneous gap nor the exact nature of the pairing glue. Nevertheless, the model enables crucial insight into several salient aspects of cuprate physics—the origin of the pseudogap and related unconventional magnetism, the universal intrinsic inhomogeneity, the nature of the strange-metal state, and superconductivity—which we briefly discuss in what follows. Notably, the myriad pseudogap features and the superconducting glue must be related to the strong correlation physics associated with the localized hole. Our simple model does not explicitly include short-range interunit cell correlations (which ought to be important for the hole localization) and should thus be viewed as coarse grained.

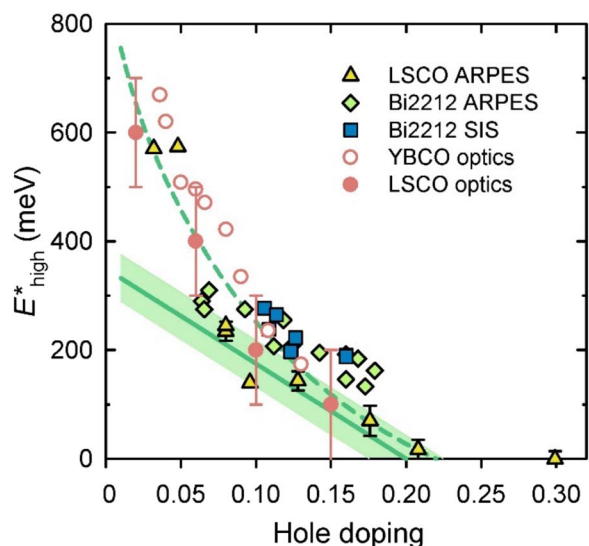


Fig. 3. Mean localization gap. Comparison of the characteristic high-energy scale for different compounds: high-energy pseudogap scale in photoemission [angle-resolved photoemission spectroscopy (ARPES)], superconductor-insulator-superconductor (SIS) tunneling spectra, and mid-infrared peak in optical conductivity data. The solid green line is our generic parameterization of the localization gap, and the shaded green band indicates the gap distribution width (Fig. 1). The dashed line is an alternative phenomenological form of the doping dependence (see Materials and Methods), which features an upward curvature and extrapolates to the transport charge-transfer gap of ~ 1 eV at zero doping (24). ARPES and SIS data for LSCO and $\text{Bi}_2\text{Sr}_2\text{CaCu}_2\text{O}_{8+\delta}$ (Bi2212) are adapted from (11); the data are from multiple experiments [see (11) for original references]. For LSCO optical conductivity peak extraction, see the Supplementary Materials. YBCO data are from (18).

Within the proposed picture, the density of itinerant carriers at the Fermi level starts to decrease upon cooling at temperatures comparable to the localization gap scale, which corresponds to the opening of local (pseudo)gaps. These temperatures are very high in underdoped compounds but approach zero at high doping. Once a significant fraction of the carriers is localized, the pseudogap is manifested in spectroscopic experiments (Fig. 3), with a characteristic energy/temperature somewhat dependent on the experimental probe (11). Since the localization is a residue of Mott physics, it will be accompanied by the emergence of antiferromagnetic correlations. Neutron scattering experiments show a distinct decrease of antiferromagnetic fluctuations above T^* (31) and a vanishing of low-energy antiferromagnetic fluctuations typically associated with local moments above $p \sim 0.28$ (32). Moreover, the universal unconventional intraunit cell magnetism (33) and related nematicity (34) below T^* might already emerge at higher temperatures along with the localization of holes, through a coupling to phonons (35) or the possible formation of loop currents (33, 36). Kerr effect measurements indicate broken time-reversal symmetry for $T < T^*$ yet show a memory effect that stems from temperatures far above T^* (37). Likewise, magnetization anisotropy measurements detect nematicity with a predetermined direction below T^* (34). This can be attributed to the broad distribution of localization energies, with incipient order at high temperatures, and T^* a lower, emergent scale. There should exist a higher emergent temperature scale T_p ($T_p > T^* > T^{**}$) where the localized holes percolate. This percolation scale may already have been observed in susceptibility and resistivity measurements on LSCO (see the Supplementary Materials).

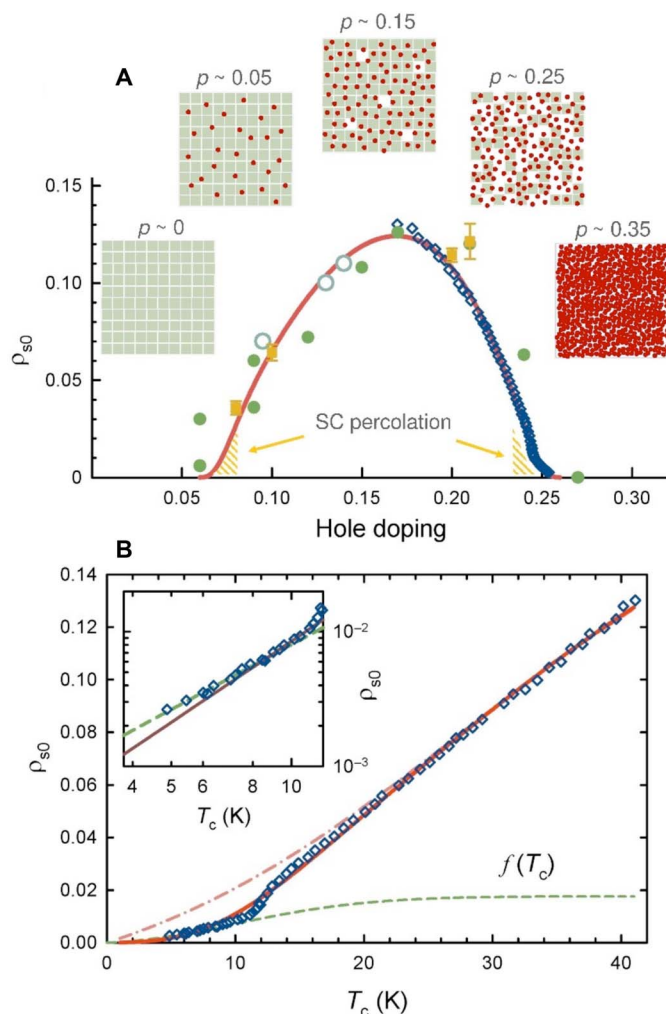


Fig. 4. Superfluid density, inhomogeneous localization, and superconducting percolation. (A) Zero-temperature superfluid density ρ_{s0} across the cuprate phase diagram calculated from Eq. 4 (orange line) and compared with experiments. The same parameters as in Figs. 1B and 2D are used ($p_c = 0.22$, $\Delta_0 = 3900$ K, $\delta = 800$ K, and $\alpha = 2$). At low doping, ρ_{s0} is limited by the density of mobile holes (red circles) and by pair-breaking impurities, whereas at high doping, the limiting factor is the density of localized holes (green squares). Diamonds are data from (17), whereas the other symbols are data for $\text{La}_{2-x}\text{Ba}_x\text{CuO}_4$ (at $p = x = 0.095$) and LSCO from optical conductivity [empty circles (97)], penetration depth [full circles (98)], and muon spin rotation [squares (51)]. The insets are schematic, and one green square represents approximately four planar CuO_2 units. A percolation regime is expected on both ends of the superconducting (SC) dome due to spatial inhomogeneity of superconducting gaps (14–16). (B) ρ_{s0} for overdoped LSCO (17) in units of holes CuO_2 units cell (blue diamonds). Between optimal doping and $T_c \sim 12$ K ($0.17 < p < 0.24$), ρ_{s0} is determined by the density of localized holes ρ_{loc} (dash-dotted line), whereas at lower T_c superconducting gap inhomogeneity causes percolation [dash-dotted green line; see Materials and Methods for the form of $f(T_c)$]. The product of the two (full line) gives a reasonable description of the entire curve. Inset: Log-log plot of ρ_{s0} at low T_c demonstrates good agreement with percolative scaling $\rho_{s0} \sim T_c^{1.6}$ (see the Supplementary Materials) (dashed dotted line) compared with the previously used quadratic scaling (full line) (17). A power-law fit $\rho_{s0} \sim T_c^\gamma$ below 9 K gives $\gamma = 1.64 \pm 0.07$.

An important feature of our model is the universal gap disorder, which might originate from either electronic correlations (38) or intrinsic structural effects (8, 9). Inhomogeneity is an intrinsic feature of many perovskites (8–10). For the cuprates, this is well documented

through structural data (8) and various direct local probes, particularly STM (12, 28), NMR (13), and x-ray absorption fine structure (see also the Supplementary Materials) (39). We emphasize that the inhomogeneity is at best weakly correlated with the level of (chemical) point disorder introduced by doping, since the model parameters are similar for LSCO and Hg1201, two cuprates with distinctly different doping chemistry and point defect severity (40). Yet, it is a distinct possibility that mechanical strain and strain accommodation associated with the perovskite-based structure are the primary causes of the gap distribution (8, 9, 39). This would result in prominent electronic features, since charge and spin degrees of freedom naturally couple to strain (and vice versa). For example, in colossal magnetoresistance manganites, strong coupling between elastic and electronic degrees of freedom is understood to be the cause of the observed multiscale inhomogeneity (41). Furthermore, recent nonlinear response experiments have found similar superconducting inhomogeneity in different perovskite-based materials that are otherwise very different (42), which indicates a common structural origin of the inhomogeneity. We find that the doping-dependent structural phase transition temperature in LSCO corresponds to nearly full charge localization ($p_{\text{loc}} \sim 98\%$), which suggests that this transition is an emergent phenomenon as well (see the Supplementary Materials and fig. S5) and that the coupling of charge carriers to the lattice is considerable. In agreement with our picture, state-of-the-art ultrafast photoemission results (43) were interpreted in terms of both correlation-induced localization physics and intrinsic inhomogeneity associated with the antinodal regions of the Fermi surface. We emphasize that ours is an effective low-energy model that packages in a simple fashion the complicated infrared (and higher energy) physics of the doped cuprates. For example, the optical spectra are complex (18, 44), and electronic correlations up to energies of several electron volts manifest themselves upon cooling below T_c (44). Lattice anharmonicity may play a role and affect the relative importance of covalent and ionic characteristics (45).

In the proposed picture, two highly unconventional features—linear- T resistivity and nonmonotonic superfluid density—originate from the same underlying gap distribution. The linear- T -like resistivity appears whenever the temperature is high enough compared with a significant fraction of the gaps. This behavior is not limited to optimal doping and is observed between $p \approx 0.05$ and $p_c \approx 0.20$, with $\rho \propto T/p$ (2, 46). Close to optimal doping, the gap distribution extends up to the Fermi energy, and thus, the linear- T -like resistivity also extends to low temperatures, again consistent with experiments (29). Because of the integration in Eq. 1, any featureless distribution will give a broad region of approximately T -linear resistivity up to temperatures determined by the distribution width ($\delta \sim 800$ K). This should be contrasted with power-law resistivity dependences due to quantum criticality, e.g., in heavy-fermion materials (47). Although often conjured to explain cuprate properties, quantum criticality results in a number of scaling laws—e.g., for the Grüneisen ratio and the dynamical spin susceptibility (47)—that have not been convincingly demonstrated, especially at the lowest temperatures/energies (29). In contrast, the existence of a universal Fermi-liquid transport scattering rate and related scaling laws are well documented throughout the phase diagram (2–5). Another possible source of linear- T resistivity was suggested to be a bad-metal incoherent transport (48), which would imply a short electronic mean-free path that violates the Mott-Ioffe-Regel limit. However, it was shown that this conventional, semiclassical limit is a serious underestimate (2, 49) and that the cuprates mostly lie in the coherent regime. As noted in (6), the experimental value of C_2 corresponds to a

room-temperature mobility of $\mu = [Hc \cot(\Theta_{\text{H}})]^{-1} \approx 10 \text{ cm}^2 \text{ V}^{-1} \text{ s}^{-1}$, which is not unusual and comparable to that of ordinary metals such as aluminum (5). Nevertheless, it is reasonable to expect deviations from simple Fermi-liquid behavior at very low doping and/or high temperatures, since other/additional scattering processes might become significant (e.g., optical phonons) or kT becomes comparable to the effective Fermi energy associated with arcs (2, 50), causing saturation (49). Our calculations demonstrate that an extended linear- T resistivity can be obtained in a simple manner, without invoking bad-metal transport or quantum criticality. However, we note that a quantum critical point associated with the emergent unconventional magnetism below T^* may well be present but, without a significant influence on transport and superconducting properties, especially at high temperatures.

The doping dependence of the superfluid density is captured using the extremely simple Eq. 2. The well-known Uemura relation $\rho_{\text{so}} \propto T_c$ for underdoped cuprates (51) directly follows from Eq. 2 if $\sigma_{\text{dc}}^{\text{res}}$ is doping independent, which for some compounds is rather well satisfied (7, 51). In contrast, $\sigma_{\text{dc}}^{\text{res}}$ of underdoped LSCO exhibits considerable doping dependence (7). The essential ingredients in the calculation of ρ_{so} are a local superconducting mechanism [as also suggested in (17)] and an underlying spatially inhomogeneous pairing strength, which naturally explains the deviations from both Leggett's theorem and Homes' law for overdoped compounds. Notably, the physical picture is in remarkable agreement with previous STM work that shows strong association between the local pairing gap and normal-state electronic correlations (28).

While our model gives an overarching picture of the normal state and captures the doping dependence of the superfluid density, it is less obvious how to treat the pairing mechanism (and thus T_c itself). Nevertheless, it is clear that the cuprate phenomenology is consistently explained by assuming two-component physics—Fermi liquid and localized—with the pairing caused by the localized component. This suggests that the mechanism belongs to the broad class of electron-electron-mediated pairing that is fast compared with the electron-phonon time scales (52). More specifically, the pairing glue is plausibly related to the mechanism first proposed by Little (53) in the context of organic conductors and, only recently, tested explicitly in a carbon nanotube system (54). This electron-electron mechanism involves (virtual) oscillations of localized charge that provide an interaction between itinerant carriers (see also the Supplementary Materials). Several experiments give evidence of the importance of oxygen-oxygen charge transfer (see the Supplementary Materials), which points to the relevance of O–Cu–O charge fluctuations (45). Qualitatively, the superconducting transition temperatures are high because of the large energy scales involved. For this pairing, the relevant energy scale should be related to the localization gap, which increases monotonically with decreasing doping, yet $T_c(p)$ is dome shaped. This can be understood by considering the experimental fact that electron-electron interactions are not instantaneous but retarded (55): For any local superconducting glue with retarded interactions, two electrons/holes must be at the same location within a given time scale. This will not occur frequently in underdoped compounds, where the carrier density is low, which leads to a decrease in T_c (see the Supplementary Materials). In overdoped compounds, the magnitude of the localization gaps decreases, which causes a concomitant decrease of T_c .

If inhomogeneous nanoscale charge localization is a generic property of perovskites, then our model could be relevant to a wide class of doped charge-transfer or Mott insulators. A Fermi-liquid scattering

rate, pseudogap effects, and nontrivial resistivity have been detected in titanates (56), whereas iridates show local gap disorder, Fermi arcs, and unconventional magnetism similar to the underdoped cuprates (57). Our model provides a unifying description of low-energy cuprate physics and captures the most relevant features of the phase diagram. All this simply follows from a spatially inhomogeneous hole (de)localization process, Fermi-liquid behavior of the itinerant (delocalized) carriers, and a local superconducting mechanism associated with the localized holes.

MATERIALS AND METHODS

Superfluid density in the percolation regime

At doping levels close to the critical values p_{c1} and p_{c2} , where bulk superconductivity disappears, we expect the underlying superconducting gap disorder [seen in temperature-dependent experiments at lower doping (14–16)] to influence the superfluid density: When the gap distribution is close to zero energy, patches of superconducting material will form in the material at $T = 0$. Quantitatively, this effect can be included into the superfluid density by modifying Eq. 2

$$\rho_{s0}^{\text{corr}} = \gamma \sigma_{\text{dc}}^{\text{res}} T_c p_{\text{loc}} f(T_c) \quad (4)$$

where the function $f(T_c)$ is the gap distribution correction. The shape of $f(T_c)$ is taken from a previous study of a diluted granular superconductor (58), where it was found that the (normalized) superfluid density is equal to the normal-state conductivity of the equivalent percolating resistor network (59). To a good approximation, the dependence of the superfluid density on the superconducting fraction (at zero temperature) is then $f = [(P - P_C)/(1 - P_C)]^\gamma$, where P is the fraction of superconducting patches, P_C the percolation threshold, and γ an exponent that depends on the dimensionality of the percolation. Note that the function f is normalized to the value at $P = 1$. To obtain the link between P and the mean T_c needed for Fig. 4, we must specify the local gap distribution function [similar to the calculations of different responses in dependence on temperature (14, 16)]. P then is the integral of the distribution function. Similar to previous work, we chose a Gaussian distribution with width Ξ_0 , leading to

$$f(T_c) = \left[\frac{1}{2(1 - P_C)} \left(1 + E \left(2 \frac{T_c}{\Xi_0} + E^{-1}(2P_C - 1) \right) - P_C \right) \right]^\gamma \quad (5)$$

where E and E^{-1} denote the direct and inverse error function, respectively. The exponents are $\gamma \approx 1.6$ and $\gamma \approx 1.0$ for three-dimensional (3D) and 2D percolation, respectively (59). The data are compatible with the 3D case (see inset of Fig. 4B), in agreement with temperature-dependent experiments that probe superconducting percolation above T_c in multiple cuprates (14–16). The corresponding critical concentration is then $P_C = 0.3$ (59).

Phase diagram and skewness of distribution

The gap distribution is usually skewed to the high-energy side (see also Supplementary Text) (12, 60). To quantify and assess the impact of this tendency, we parametrized the distribution as a Gaussian multiplied by its integral

$$g(\Delta, \Delta_p, \delta) = 2\phi(\Delta, \Delta_p, \delta) \int_{-\infty}^{\alpha\Delta} \phi(\Delta', \Delta_p, \delta) d\Delta' \quad (6)$$

where α is a dimensionless parameter that controls the skewness of the distribution, and ϕ is a normalized Gaussian distribution with mean Δ_p and full width at half maximum δ . The skewness can be continuously varied by changing α . For $\alpha = 0$, the distribution reduces to a simple Gaussian.

In fig. S1, we tested different values of the skew parameter and different functional forms for the gap distribution to demonstrate that this yields essentially the same phase diagrams. The main features are rather insensitive to the choice of distribution shape, mainly due to the fact that the resistivity calculation involves an integral over energy. Along with skewed Gaussians, we tested a shifted gamma distribution that features a heavier tail at high energies and gives a broader linear- T resistivity region on the overdoped side of the phase diagram.

Choice of doping dependences of distribution parameters

The simplest assumption of a linear decrease of the mean energy and doping-independent distribution width may be relaxed by introducing additional parameters and assumptions. While these assumptions are purely phenomenological (and detract somewhat from the main message of the simplest possible calculation), an eventual microscopic theory should be capable of providing the true doping dependences, at least in principle. To test the robustness of our calculation, we introduced a curvature into the dependence of the mean gap on doping, using the function of the form

$$\Delta_p(p) = \Delta_0 [1 - \tanh(p/p_c)/\tanh(1)] \quad (7)$$

This function still crosses zero at $p = p_c$ (and contains no additional parameters) but has an upward curvature at higher doping. A similar function can be used for the dependence of the distribution width on doping, but with a more general form

$$\delta(p) = \delta_0 [1 - \beta \tanh(p/p_c)] \quad (8)$$

where β is a numerical constant. The more constrained form with $\beta = 1/\tanh(1)$ cannot be used for δ , since it would lead to a zero distribution width at p_c and nonphysical divergences in the calculations. We chose $\beta \sim 0.4$, but again, it turned out that the exact value is not very important. The main features of the phase diagram were unchanged, but introducing these nontrivial doping dependences of Δ_p and δ somewhat broadened the region of the phase diagram where the resistivity is linear in temperature on the overdoped side (fig. S2). To introduce curvature in $\Delta_p(p)$ at low doping, in line with some experiments (Fig. 3 in the main text), we further modified Eq. 7 and cast it in the form

$$\Delta_p(p) = \Delta_0 \left[1 - (\tanh(p/p_c)/\tanh(1))^{1/2} \right] \quad (9)$$

without introducing additional free parameters. This form gives better agreement between calculated and measured Hall coefficients for strongly underdoped LSCO (see the Supplementary Materials), as well as a better match between the modeled mean energy (dashed line in Fig. 3) and the characteristic high-energy scale from experiments. Moreover, it has the physically appealing feature that Δ_0 is approximately 1 eV, the charge-transfer gap at zero doping as determined from Hall-effect measurements (24). Yet again, this introduces no considerable changes to the overall picture.

SUPPLEMENTARY MATERIALS

Supplementary material for this article is available at <http://advances.sciencemag.org/cgi/content/full/5/1/eaau4538/DC1>

Supplementary Text

Fig. S1. Normal-state phase diagram for different gap distributions.

Fig. S2. Normal-state phase diagrams for two doping dependences of the gap distribution parameters.

Fig. S3. Local probes of disorder in cuprates.

Fig. S4. High-energy gap scale in cuprates.

Fig. S5. Characteristic temperature and localization.

Fig. S6. Temperature and doping dependence of Hall constant for LSCO.

Fig. S7. Doping dependence of linear and quadratic resistivity coefficients of LSCO.

Fig. S8. Doping dependence of sheet resistance coefficients.

References (61–96)

REFERENCES AND NOTES

- B. Keimer, S. A. Kivelson, M. R. Norman, S. Uchida, J. Zaanen, From quantum matter to high-temperature superconductivity in copper oxides. *Nature* **518**, 179–186 (2015).
- N. Barišić, M. K. Chan, Y. Li, G. Yu, X. Zhao, M. Dressel, A. Smontara, M. Greven, Universal sheet resistance and revised phase diagram of the cuprate high-temperature superconductors. *Proc. Natl. Acad. Sci. U.S.A.* **110**, 12235–12240 (2013).
- S. I. Mirzaei, D. Stricker, J. N. Hancock, C. Berthod, A. Georges, E. van Heumen, M. K. Chan, X. Zhao, Y. Li, M. Greven, N. Barišić, D. van der Marel, Spectroscopic evidence for Fermi-liquid-like energy and temperature dependence of the relaxation rate in the pseudogap phase of the cuprates. *Proc. Natl. Acad. Sci. U.S.A.* **110**, 5774–5778 (2013).
- M. K. Chan, M. J. Veit, C. J. Dorow, Y. Ge, Y. Li, W. Tabis, Y. Tang, X. Zhao, N. Barišić, M. Greven, In-plane magnetoresistance obeys Kohler's rule in the pseudogap phase of cuprate superconductors. *Phys. Rev. Lett.* **113**, 177005 (2014).
- N. Barišić, M. K. Chan, M. J. Veit, C. J. Dorow, Y. Ge, Y. Tang, W. Tabis, G. Yu, X. Zhao, M. Greven, Hidden Fermi liquid behavior throughout the phase diagram of the cuprates. [arXiv:1507.07885](https://arxiv.org/abs/1507.07885) [cond-mat.supr-con] (28 July 2015).
- Y. Li, W. Tabis, G. Yu, N. Barišić, M. Greven, Hidden Fermi-liquid charge transport in the antiferromagnetic phase of the electron-doped cuprate superconductors. *Phys. Rev. Lett.* **117**, 197001 (2016).
- Y. Ando, S. Komiya, K. Segawa, S. Ono, Y. Kurita, Electronic phase diagram of high- T_c cuprate superconductors from a mapping of the in-plane resistivity curvature. *Phys. Rev. Lett.* **93**, 267001 (2004).
- J. A. Krumhansl, Fine scale mesostructures in superconducting and other materials, in *Proceedings of the Conference of the Lattice Effects in High- T_c Superconductors*, 13 to 15 January 1992 (World Scientific, 1992).
- J. C. Phillips, A. Saxena, A. R. Bishop, Pseudogaps, dopands, and strong disorder in cuprate high-temperature superconductors. *Rep. Prog. Phys.* **66**, 2111–2182 (2003).
- E. Dagotto, Complexity in strongly correlated electronic systems. *Science* **309**, 257–262 (2005).
- T. Honma, P. H. Hor, Unified electronic phase diagram for hole-doped high- T_c cuprates. *Phys. Rev. B* **77**, 184520 (2008).
- J. W. Allredge, K. Fujita, H. Eisaki, S. Uchida, K. McElroy, Universal disorder in $\text{Bi}_2\text{Sr}_2\text{CaCu}_2\text{O}_{8+x}$. *Phys. Rev. B* **87**, 104520 (2013).
- P. M. Singer, A. W. Hunt, T. Imai, ^{63}Cu NQR evidence for spatial variation of hole concentration in $\text{La}_{2-x}\text{Sr}_x\text{CuO}_4$. *Phys. Rev. Lett.* **88**, 047602 (2002).
- D. Pelc, M. Vučković, M. Grbić, M. Požek, G. Yu, T. Sasagawa, M. Greven, N. Barišić, Emergence of superconductivity in the cuprates via a universal percolation process. *Nat. Commun.* **9**, 4327 (2018).
- G. Yu, D.-D. Xia, D. Pelc, R.-H. He, N.-H. Kaneko, T. Sasagawa, Y. Li, X. Zhao, N. Barišić, A. Shekhter, M. Greven, Universal superconducting precursor in the cuprates. [arXiv:1710.10957](https://arxiv.org/abs/1710.10957) [cond-mat.supr-con] (27 October 2017).
- P. Popčević, D. Pelc, Y. Tang, K. Velebit, Z. Anderson, V. Nagarajan, G. Yu, M. Požek, N. Barišić, M. Greven, Percolative nature of the dc paraconductivity in the cuprate superconductors. *npj Quant. Mater.* **3**, 42 (2018).
- I. Božović, X. He, J. Wu, A. T. Bollinger, Dependence of the critical temperature in overdoped copper oxides on superfluid density. *Nature* **536**, 309–311 (2016).
- Y. S. Lee, K. Segawa, Z. Q. Li, W. J. Padilla, M. Dumm, S. V. Dordevic, C. C. Homes, Y. Ando, D. N. Basov, Electrodynamics of the nodal metal state in weakly doped high- T_c cuprates. *Phys. Rev. B* **72**, 054529 (2005).
- J. Haase, D. Rybicki, C. P. Slichter, M. Greven, G. Yu, Y. Li, X. Zhao, Two-component uniform spin susceptibility of superconducting $\text{HgBa}_2\text{CuO}_{4+\delta}$ single crystals measured using ^{63}Cu and ^{199}Hg nuclear magnetic resonance. *Phys. Rev. B* **85**, 104517 (2012).
- T. Meissner, S. K. Goh, J. Haase, G. V. M. Williams, P. B. Littlewood, High-pressure spin shifts in the pseudogap regime of superconducting $\text{YBa}_2\text{Cu}_3\text{O}_8$ as revealed by ^{17}O NMR. *Phys. Rev. B* **83**, 220519 (2011).
- J. G. Storey, J. L. Tallon, Two-component electron fluid in underdoped high- T_c cuprate superconductors. *Europhys. Lett.* **98**, 17011 (2012).
- I. K. Drozdov, I. Pletikosić, C.-K. Kim, K. Fujita, G. D. Gu, J. C. Seamus Davis, P. D. Johnson, I. Božović, T. Valla, Phase diagram of $\text{Bi}_2\text{Sr}_2\text{CaCu}_2\text{O}_{8+\delta}$ revisited. *Nat. Commun.* **9**, 5210 (2018).
- L. P. Gor'kov, G. B. Teitelbaum, Interplay of externally doped and thermally activated holes in $\text{La}_{2-x}\text{Sr}_x\text{CuO}_4$ and their impact on the pseudogap crossover. *Phys. Rev. Lett.* **97**, 247003 (2006).
- S. Ono, S. Komiya, Y. Ando, Strong charge fluctuations manifested in the high-temperature Hall coefficient of high- T_c cuprates. *Phys. Rev. B* **75**, 024515 (2007).
- S. Nakamae, K. Behnia, N. Mangkorntong, M. Nohara, H. Takagi, S. J. C. Yates, N. E. Hussey, Electronic ground state of heavily overdoped nonsuperconducting $\text{La}_{2-x}\text{Sr}_x\text{CuO}_4$. *Phys. Rev. B* **68**, 100502 (2003).
- C. Proust, B. Vignolle, J. Levallois, S. Adachi, N. E. Hussey, Fermi liquid behavior of the in-plane resistivity in the pseudogap state of $\text{YBa}_2\text{Cu}_3\text{O}_8$. *Proc. Natl. Acad. Sci. U.S.A.* **113**, 13654–13659 (2016).
- C. C. Homes, S. V. Dordevic, T. Valla, M. Strongin, Scaling of the superfluid density in high-temperature superconductors. *Phys. Rev. B* **72**, 134517 (2005).
- A. N. Pasupathy, A. Pushp, K. K. Gomes, C. V. Parker, J. Wen, Z. Xu, G. Gu, S. Ono, Y. Ando, A. Yazdani, Electronic origin of the inhomogeneous pairing interaction in the high- T_c superconductor $\text{Bi}_2\text{Sr}_2\text{CaCu}_2\text{O}_{8+\delta}$. *Science* **320**, 196–201 (2008).
- R. A. Cooper, Y. Wang, B. Vignolle, O. J. Lipscombe, S. M. Hayden, Y. Tanabe, T. Adachi, Y. Koike, M. Nohara, H. Takagi, C. Proust, N. E. Hussey, Anomalous criticality in the electrical resistivity of $\text{La}_{2-x}\text{Sr}_x\text{CuO}_4$. *Science* **323**, 603–607 (2009).
- X. Leng, J. Garcia-Barriocanal, S. Bose, Y. Lee, A. M. Goldman, Electrostatic control of the evolution from a superconducting phase to an insulating phase in ultrathin $\text{YBa}_2\text{Cu}_3\text{O}_{7-x}$ films. *Phys. Rev. Lett.* **107**, 027001 (2011).
- M. K. Chan, C. J. Dorow, L. Mangin-Thro, Y. Tang, Y. Ge, M. J. Veit, G. Yu, X. Zhao, A. D. Christianson, J. T. Park, Y. Sidis, P. Steffens, D. L. Abernathy, P. Bourges, M. Greven, Commensurate antiferromagnetic excitations as a signature of the pseudogap in the tetragonal high- T_c cuprate $\text{HgBa}_2\text{CuO}_{4+\delta}$. *Nat. Commun.* **7**, 10819 (2016).
- S. Wakimoto, H. Zhang, K. Yamada, I. Swainson, H. Kim, R. J. Birgeneau, Direct relation between the low-energy spin excitations and superconductivity of overdoped high- T_c superconductors. *Phys. Rev. Lett.* **92**, 217004 (2004).
- Y. Li, V. Balédent, N. Barišić, Y. Cho, B. Fauqué, Y. Sidis, G. Yu, X. Zhao, P. Bourges, M. Greven, Unusual magnetic order in the pseudogap region of the superconductor $\text{HgBa}_2\text{CuO}_{4+\delta}$. *Nature* **455**, 372–375 (2008).
- H. Murayama, Y. Sato, R. Kurihara, S. Kasahara, Y. Mizukami, Y. Kasahara, H. Uchiyama, A. Yamamoto, E.-G. Moon, J. Cai, J. Freyermuth, M. Greven, T. Shibauchi, Y. Matsuda, Diagonal nematicity in the pseudogap phase of $\text{HgBa}_2\text{CuO}_{4+\delta}$. [arXiv:1805.00276](https://arxiv.org/abs/1805.00276) [cond-mat.supr-con] (1 May 2018).
- M. Fechner, M. J. A. Fierz, F. Thöle, U. Staub, N. A. Spaldin, Quasistatic magnetoelectric multipoles as order parameter for pseudogap phase in cuprate superconductors. *Phys. Rev. B* **93**, 174419 (2016).
- C. M. Varma, Non-Fermi-liquid states and pairing instability of a general model of copper oxide metals. *Phys. Rev. B* **55**, 14554–14580 (1997).
- J. Xia, E. Schemm, G. Deutscher, S. A. Kivelson, D. A. Bonn, W. N. Hardy, R. Liang, W. Siemons, G. Koster, M. M. Fejer, A. Kapitulnik, Polar Kerr effect measurements of the high-temperature $\text{YBa}_2\text{Cu}_3\text{O}_{6+x}$ superconductor: Evidence for broken symmetry near the pseudogap temperature. *Phys. Rev. Lett.* **100**, 127002 (2008).
- V. J. Emery, S. A. Kivelson, H. Q. Lin, Phase separation in the t - J model. *Phys. Rev. Lett.* **64**, 475–478 (1990).
- N. L. Saini, A. Bianconi, H. Oyanagi, Evidence for critical lattice fluctuations in the high- T_c cuprates. *J. Phys. Soc. Jpn.* **70**, 2092–2097 (2001).
- H. Eisaki, N. Kaneko, D. L. Feng, A. Damascelli, P. K. Mang, K. M. Shen, Z.-X. Shen, M. Greven, Effect of chemical inhomogeneity in bismuth-based copper oxide superconductors. *Phys. Rev. B* **69**, 064512 (2004).
- K. H. Ahn, T. Lookman, A. R. Bishop, Strain-induced metal-insulator phase coexistence in perovskite manganites. *Nature* **428**, 401–404 (2004).
- D. Pelc, Z. Anderson, B. Yu, C. Leighton, M. Greven, Universal superconducting precursor in perovskite-based oxides. [arXiv:1808.05763](https://arxiv.org/abs/1808.05763) [cond-mat.supr-con] (17 August 2018).
- F. Cilento, G. Manzoni, A. Sterzi, S. Peli, A. Ronchi, A. Crepaldi, F. Boschini, C. Cacho, R. Chapman, E. Springate, H. Eisaki, M. Greven, M. Berciu, A. F. Kemper, A. Damascelli, M. Capone, C. Giannetti, F. Parmigiani, Dynamics of correlation-frozen antinodal quasiparticles in superconducting cuprates. *Sci. Adv.* **4**, eaar1998 (2018).
- E. van Heumen, E. Muhlethaler, A. B. Kuzmenko, H. Eisaki, W. Meevasana, M. Greven, D. van der Marel, Optical determination of the relation between the electron-boson coupling function and the critical temperature in high- T_c cuprates. *Phys. Rev. B* **79**, 184512 (2009).
- S. Barišić, O.-S. Barišić, Approaching large U_d high- T_c cuprates from the covalent side. *J. Supercond. Nov. Magn.* **25**, 669–676 (2012).

46. H. Takagi, B. Batlogg, H. L. Kao, J. Kwo, R. J. Cava, J. J. Krajewski, W. F. Peck Jr., Systematic evolution of temperature-dependent resistivity in $\text{La}_{2-x}\text{Sr}_x\text{CuO}_4$. *Phys. Rev. Lett.* **69**, 2975–2978 (1992).
47. P. Gegenwart, Q. Si, F. Steglich, Quantum criticality in heavy-fermion metals. *Nat. Phys.* **4**, 186–197 (2008).
48. S. A. Hartnoll, Theory of universal incoherent metallic transport. *Nat. Phys.* **11**, 54–61 (2014).
49. O. Gunnarson, M. Calandra, J. E. Han, Saturation of electrical resistivity. *Rev. Mod. Phys.* **75**, 1085 (2003).
50. M. Oda, R. M. Distaso, M. Momono, M. Ido, Hyperbolic dependence of $2\Delta_0$ vs. T_c ratio on hole-doping level in high- T_c cuprates: Energy scale in determining T_c . *J. Phys. Soc. Jpn.* **69**, 983–984 (2000).
51. Y. J. Uemura, L. P. Le, G. M. Luke, B. J. Sternlieb, W. D. Wu, J. H. Brewer, T. M. Riseman, C. L. Seaman, M. B. Maple, M. D. G. Hinks, J. D. Jorgensen, G. Saito, H. Yamochi, Basic similarities between cuprate, bismuthate, organic, Chevrel-phase and heavy fermion superconductors shown by penetration depth measurements. *Phys. Rev. Lett.* **66**, 2665–2668 (1992).
52. R. Micnas, J. Ranninger, S. Robaszkiewicz, Superconductivity in narrow-band systems with local nonretarded attractive interactions. *Rev. Mod. Phys.* **62**, 113–171 (1990).
53. W. A. Little, A look back at an innocent question first proposed fifty years ago. *J. Supercond. Novel Magn.* **29**, 3–8 (2016).
54. A. Hamo, A. Benyamini, I. Shapir, I. Khivrich, J. Waissman, K. Kaasbjerg, Y. Oreg, F. von Oppen, S. Ilani, Electron attraction mediated by Coulomb repulsion. *Nature* **535**, 395–400 (2016).
55. S. Dal Conte, L. Vidmar, D. Golež, M. Mierzejewski, G. Soavi, S. Peli, F. Banfi, G. Ferrini, R. Comin, B. M. Ludbrook, L. Chauviere, N. D. Zhigadlo, H. Eisaki, M. Greven, S. Lupi, A. Damascelli, D. Brida, M. Capone, J. Bonča, G. Cerullo, C. Giannetti, Snapshots of the retarded interaction of charge carriers with ultrafast fluctuations in cuprates. *Nat. Phys.* **11**, 421–426 (2015).
56. E. Mikheev, C. R. Freeze, B. J. Isaac, T. A. Cain, S. Stemmer, Separation of transport lifetimes in SrTiO_3 -based two-dimensional electron liquids. *Phys. Rev. B* **91**, 165125 (2015).
57. I. Battisti, K. M. Bastiaans, V. Fedoseev, A. de la Torre, N. Iliopoulos, A. Tamai, E. C. Hunter, R. S. Perry, J. Zaanen, F. Baumberg, M. P. Allan, Universality of pseudogap and emergent order in lightly doped Mott insulators. *Nat. Phys.* **13**, 21–25 (2017).
58. C. Ebner, D. Stroud, Superfluid density, penetration depth, and integrated fluctuation conductivity of a model granular superconductor. *Phys. Rev. B* **28**, 5053–5060 (1983).
59. S. Kirkpatrick, Percolation and conduction. *Rev. Mod. Phys.* **45**, 574–588 (1973).
60. K. K. Gomes, A. N. Pasupathy, A. Pushp, S. Ono, Y. Ando, A. Yazdani, Visualizing pair formation on the atomic scale in the high- T_c superconductor $\text{Bi}_2\text{Sr}_2\text{CaCu}_2\text{O}_{8+\delta}$. *Nature* **447**, 569–572 (2007).
61. M. C. Boyer, W. D. Wise, K. Chatterjee, M. Yi, T. Kondo, T. Takeuchi, H. Ikuta, E. W. Hudson, Imaging the two gaps in the high-temperature superconductor $\text{Bi}_2\text{Sr}_2\text{CuO}_{6+x}$. *Nat. Phys.* **3**, 802–806 (2007).
62. D. Rybicki, J. Haase, M. Greven, G. Yu, Y. Li, Y. Cho, X. Zhao, Spatial inhomogeneities in single-crystal $\text{HgBa}_2\text{CuO}_{4+\delta}$ from ^{63}Cu NMR spin and quadrupole shifts. *J. Supercond. Novel Magn.* **22**, 179–183 (2009).
63. S. Ohsugi, Y. Kitaoka, K. Ishida, G.-Q. Zheng, K. Asayama, Cu NMR and NQR studies of high- T_c superconductor. $\text{La}_{2-x}\text{Sr}_x\text{CuO}_4$. *J. Phys. Soc. Jpn.* **63**, 700–715 (1994).
64. J. Brobroff, H. Alloul, S. Ouazi, P. Mendels, A. Mahajan, N. Blanchard, G. Collin, V. Guillen, J.-F. Marucco, Absence of static phase separation in the high- T_c cuprate $\text{YBa}_2\text{Cu}_3\text{O}_{6+y}$. *Phys. Rev. Lett.* **89**, 157002 (2002).
65. D.-H. Lee, S. A. Kivelson, Two classes of Mott insulator. *Phys. Rev. B* **67**, 024506 (2003).
66. F. V. Kusmartsev, M. Saarela, About two-component physics of HTSC. *J. Supercond. Novel Magn.* **22**, 155–163 (2009).
67. N. Fratini, N. Poccia, A. Ricci, G. Campi, M. Burghammer, G. Aeppli, A. Bianconi, Scale-free structural organisation of oxygen interstitials in $\text{La}_2\text{CuO}_{4+\delta}$. *Nature* **466**, 841–844 (2010).
68. J. W. Halley, X.-F. Wang, S. Davis, Mean field calculations of the properties of the dilute t-J model for high- T_c superconductivity. *Phys. Rev. B* **46**, 6560–6571 (1992).
69. J. C. Phillips, Percolative theories of strongly disordered ceramic high-temperature superconductivity. *Proc. Natl. Acad. Sci. U.S.A.* **107**, 1307–1310 (2010).
70. W. F. Brinkman, T. M. Rice, Electron-hole liquids in semiconductors. *Phys. Rev. B* **7**, 1508–1523 (1973).
71. W. D. Wise, M. C. Boyer, K. Chatterjee, T. Kondo, T. Takeuchi, H. Ikuta, Y. Wang, E. W. Hudson, Charge-density-wave origin of cuprate checkerboard visualized by scanning tunnelling microscopy. *Nat. Phys.* **4**, 696–699 (2008).
72. R. Comin, A. Frano, M. M. Yee, Y. Yoshida, H. Eisaki, E. Schierle, E. Weschke, R. Sutarto, F. He, A. Soumyanarayanan, Y. He, M. Le Tacon, I. S. Elfimov, J. E. Hoffman, G. A. Sawatzky, B. Keimer, A. Damascelli, Charge order driven by Fermi-arc instability in $\text{Bi}_2\text{Sr}_{2-x}\text{La}_x\text{CuO}_{6+\delta}$. *Science* **343**, 390–392 (2014).
73. E. H. da Silva Neto, P. Aynajian, A. Frano, R. Comin, E. Schierle, E. Weschke, A. Gyenis, J. Wen, J. Schneeloch, Z. Xu, S. Ono, G. Gu, M. Le Tacon, A. Yazdani, Ubiquitous interplay between charge ordering and high-temperature superconductivity in cuprates. *Science* **343**, 393–396 (2014).
74. G. Blumberg, M. Kang, M. V. Klein, K. Kadowaki, C. Kendziora, Evolution of magnetic and superconducting fluctuations with doping of high- T_c superconductors. *Science* **278**, 1427–1432 (1997).
75. S. Uchida, T. Ido, H. Takagi, T. Arima, Y. Tokura, S. Tajima, Optical spectra of $\text{La}_{2-x}\text{Sr}_x\text{CuO}_4$: Effect of carrier doping on the electronic structure of the CuO_2 plane. *Phys. Rev. B* **43**, 7942–7954 (1991).
76. M. R. Norman, H. Ding, J. C. Campuzano, T. Takeuchi, M. Randeria, T. Yokoya, T. Takahashi, T. Mochiku, K. Kadowaki, Unusual dispersion and line shape of the superconducting state spectra of $\text{Bi}_2\text{Sr}_2\text{CaCu}_2\text{O}_{8+\delta}$. *Phys. Rev. Lett.* **79**, 3506–3509 (1997).
77. A. Damascelli, Z. Hussain, Z.-X. Shen, Angle-resolved photoemission studies of the cuprate superconductors. *Rev. Mod. Phys.* **75**, 473–541 (2003).
78. D. Mandrus, L. Forro, D. Koller, L. Mihaly, Giant tunneling anisotropy in the high- T_c superconductor $\text{Bi}_2\text{Sr}_2\text{CaCu}_2\text{O}_8$. *Nature* **351**, 460–462 (1991).
79. L. Ozyuzer, J. F. Zasadzinski, C. Kendziora, K. E. Gray, Quasiparticle and Josephson tunneling of overdoped $\text{Bi}_2\text{Sr}_2\text{CaCu}_2\text{O}_{8+\delta}$. *Phys. Rev. B* **61**, 3629–3640 (2000).
80. N. Luo, G. H. Miley, An alternative theory on relaxation rates in cuprate superconductors. *J. Phys. Condens. Matter* **21**, 025701 (2009).
81. T. Honma, P. H. Hor, Quantitative connection between the nanoscale electronic inhomogeneity and the pseudogap of $\text{Bi}_2\text{Sr}_2\text{CaCu}_2\text{O}_{8+\delta}$ superconductors. *Phys. C* **509**, 11–15 (2015).
82. B. Keimer, N. Belk, R. J. Birgeneau, A. Cassanho, C. Y. Chen, M. Greven, M. A. Kastner, A. Aharony, Y. Endoh, R. W. Erwin, G. Shirane, Magnetic excitations in pure, lightly doped and weakly metallic La_2CuO_4 . *Phys. Rev. B* **46**, 14034–14053 (1992).
83. H. Y. Hwang, B. Batlogg, H. Takagi, H. L. Kao, J. Kwo, R. J. Cava, J. J. Krajewski, W. F. Peck Jr., Scaling of the temperature dependent Hall effect in $\text{La}_{2-x}\text{Sr}_x\text{CuO}_4$. *Phys. Rev. Lett.* **72**, 2636–2639 (1994).
84. Y. Ando, Y. Kurita, S. Komiyama, S. Ono, K. Segawa, Evolution of the Hall coefficient and the peculiar electronic structure of cuprate superconductors. *Phys. Rev. Lett.* **92**, 197001 (2004).
85. Y. Kubo, T. Manako, T^2 -dependence of inverse Hall mobility observed in overdoped Ti -cuprates. *Phys. C* **197**, 378–384 (1992).
86. N. Luo, G. H. Miley, Kohler's rule and relaxation rates in high- T_c superconductors. *Phys. C* **371**, 259–269 (2002).
87. A. Ino, C. Kim, M. Nakamura, T. Yoshida, T. Mizokawa, A. Fujimori, Z.-X. Shen, T. Kakeshita, H. Eisaki, S. Uchida, Doping-dependent evolution of the electronic structure of $\text{La}_{2-x}\text{Sr}_x\text{CuO}_4$ in the superconducting and metallic phases. *Phys. Rev. B* **65**, 094504 (2002).
88. T. M. Rice, N. J. Robinson, A. M. Tselvelik, Umklapp scattering as the origin of T -linear resistivity in the normal state of high- T_c cuprates. *Phys. Rev. B* **96**, 220502 (2017).
89. W. L. McMillan, Transition temperature of strong-coupled superconductors. *Phys. Rev.* **167**, 331–344 (1968).
90. P. Morel, P. W. Anderson, Calculation of the superconducting state parameters with retarded electron-phonon interaction. *Phys. Rev.* **125**, 1263–1271 (1962).
91. A. B. Migdal, Interaction between electrons and lattice vibrations in a normal metal. *Zh. Eksp. Theor. Fiz.* **34**, 1438–1443 (1958).
92. G. Seibold, L. Benfatto, C. Castellani, J. Lorenzana, Superfluid density and phase relaxation in superconductors with strong disorder. *Phys. Rev. Lett.* **108**, 207004 (2012).
93. B. Büchner, M. Breuer, A. Freimuth, A. P. Kampf, Critical buckling for the disappearance of superconductivity in rare-earth-doped $\text{La}_{2-x}\text{Sr}_x\text{CuO}_4$. *Phys. Rev. Lett.* **73**, 1841–1844 (1994).
94. D. Pelc, M. Požek, V. Despoja, D. K. Sunko, Mechanism of metallization and superconductivity suppression in $\text{YBa}_2(\text{Cu}_{0.97}\text{Zn}_{0.03})_3\text{O}_{6.92}$ revealed by ^{67}Zn NQR. *New J. Phys.* **17**, 083033 (2015).
95. R. Comin, R. Sutarto, F. He, E. H. da Silva Neto, L. Chauviere, A. Frañó, R. Liang, W. N. Hardy, D. A. Bonn, Y. Yoshida, H. Eisaki, A. J. Achkar, D. G. Hawthorn, B. Keimer, G. A. Sawatzky, A. Damascelli, Symmetry of charge order in cuprates. *Nat. Mater.* **14**, 796–800 (2015).
96. S. Barišić, J. Zelenko, Electron mechanism for the structural phase transitions in $\text{La}_{2-x}\text{Ba}_x\text{CuO}_4$. *Solid State Commun.* **74**, 367–370 (1990).
97. C. C. Homes, M. Hücker, Q. Li, Z. J. Xu, J. S. Wen, G. D. Gu, J. M. Tranquada, Determination of the optical properties of $\text{La}_{2-x}\text{Ba}_x\text{CuO}_4$ for several dopings, including the anomalous $x = 1/8$ phase. *Phys. Rev. B* **85**, 134510 (2012).
98. T. R. Lemberger, I. Hetel, A. Tsukada, M. Naito, M. Randeria, Superconductor-to-metal quantum phase transition in overdoped $\text{La}_{2-x}\text{Sr}_x\text{CuO}_4$. *Phys. Rev. B* **83**, 140507 (2011).

Acknowledgments: N.B. is grateful to the late S. Barišić for extensive discussions. We wish to acknowledge J. M. Tranquada and G. Yu for helpful comments on the manuscript. **Funding:** D.P. and M.P. acknowledge funding by the Croatian Science Foundation under grant no. IP-2018-01-2970. P.P. acknowledges funding by the Croatian Science Foundation under grant no. IP-2016-06-7258. The work at the University of Minnesota was funded by the Department of Energy through the University of Minnesota Center for Quantum Materials under DE-SC-0016371. The work at the TU Wien was supported by FWF project P27980-N36 and the European

Research Council (ERC Consolidator Grant no. 725521). **Author contributions:** D.P., M.G., and N.B. conceived the model. D.P. and P.P. performed the calculations and analyzed the data. M.P., M.G., and N.B. supervised the research. D.P., M.G., and N.B. wrote the manuscript with input from all the other authors. **Competing interests:** All authors declare that they have no competing interests. **Data and materials availability:** All data needed to evaluate the conclusions are present in the paper and/or the Supplementary Materials. Additional data related to this paper may be requested from the authors.

Submitted 12 June 2018
Accepted 7 December 2018
Published 25 January 2019
10.1126/sciadv.aau4538

Citation: D. Pelc, P. Popčević, M. Požek, M. Greven, N. Barišić, Unusual behavior of cuprates explained by heterogeneous charge localization. *Sci. Adv.* **5**, eaau4538 (2019).

Unusual behavior of cuprates explained by heterogeneous charge localization

D. Pelc, P. Popcevic, M. Pozek, M. Greven and N. Barisic

Sci Adv **5** (1), eaau4538.

DOI: 10.1126/sciadv.aau4538

ARTICLE TOOLS

<http://advances.sciencemag.org/content/5/1/eaau4538>

SUPPLEMENTARY MATERIALS

<http://advances.sciencemag.org/content/suppl/2019/01/18/5.1.eaau4538.DC1>

REFERENCES

This article cites 93 articles, 11 of which you can access for free
<http://advances.sciencemag.org/content/5/1/eaau4538#BIBL>

PERMISSIONS

<http://www.sciencemag.org/help/reprints-and-permissions>

Use of this article is subject to the [Terms of Service](#)

Science Advances (ISSN 2375-2548) is published by the American Association for the Advancement of Science, 1200 New York Avenue NW, Washington, DC 20005. The title *Science Advances* is a registered trademark of AAAS.

Copyright © 2019 The Authors, some rights reserved; exclusive licensee American Association for the Advancement of Science. No claim to original U.S. Government Works. Distributed under a Creative Commons Attribution NonCommercial License 4.0 (CC BY-NC).